JOM, Vol. 74, No. 11, 2022
https://doi.org/10.1007/s11837-022-05377-y

Microstructure and Mechanical Properties of In-Situ B4C-(TiZrHfNbTa) B2 Composite by Reactive Spark Plasma Sintering

DONG WANG,[1,2,4] KAI XU,[2] QINGGUI LI,[3] XIANG DING,[3] and SONGLIN RAN[3,5]

1.—Key Laboratory of Green Fabrication and Surface Technology of Advanced Metal Materials, Ministry of Education, Anhui University of Technology, Ma'anshan 243002, China. 2.—School of Materials Science and Engineering, Anhui University of Technology, Ma'anshan 243002, China. 3.—Anhui Province Key Laboratory of Metallurgical Engineering & Resources Recycling, Anhui University of Technology, Ma'anshan 243002, China. 4.—e-mail: dongwang@ahut.edu.cn. 5.—e-mail: ransonglin@ahut.edu.cn

B_4C-45vol.% (TiZrHfNbTa) B_2 composite was prepared by in-situ reactive spark plasma sintering at 2000°C using powders of transition metal carbides and amorphous boron as raw materials. The composite reached a relative density of over 97% Within 6 min. The simultaneously generated B_4C and (TiZrHfNbTa) B_2 phases had homogeneous microstructures with particle sizes ~ 1 μm, and Nb segregations in (TiZrHfNbTa) B_2 grains were detected. The composite obtained a high three-point bending strength of 422 MPa, a Vickers hardness of 20.9 GPa and a fracture toughness of 5.48 MPa $m^{1/2}$, respectively. The fine grain and solid solution effects are the main reasons for the improved properties. The crack deflection, branching, and bridging mechanisms observed are also helpful for an improved fracture toughness of the composite. This work provides a fast, convenient method of preparing novel B_4C high-entropy boride composite ceramics with enhanced properties.

INTRODUCTION

The advantages of a high melting point (2450°C), high hardness, low density (2.52 g cm^{-3}), high neutron absorption cross section, and good wear resistance make boron carbide (B_4C) a promising candidate for use in aerospace, bulletproof armor plates, neutron absorbers, and some engineering wear-resistant parts. However, the application of B_4C is limited due to difficulties in densification, low fracture toughness (2.2 MPa $m^{1/2}$), and low oxidation resistance.[1–3] To overcome these disadvantages, secondary phases, such as carbides (SiC, TiC), oxides (Al_2O_3, ZrO_2), and transition metal diborides (TMB_2s, TiB_2, ZrB_2), are usually added to achieve better sintering ability, superior mechanical properties and oxidation resistance.[4–9]

(Received December 14, 2021; accepted May 27, 2022; published online June 16, 2022)

Compared with individual TMB_2s, the new emerging high-entropy transition metal borides (HEBs) have greater hardness, better oxidation resistance, and unique electrochemical performance, which are promising in the family of ultra-high-temperature ceramics (UHTCs).[10–16] Moreover, the HEBs are much more designable. By adjusting the composition and microstructure of HEBs, it is possible to control the thermal-physical and mechanical properties, and they could be more compatible with B_4C than individual TMB_2s. The B_4C-HEB composites are therefore attractive for a combination of high hardness, low density, and designability, which could be useful for personal and lightweight armor systems and other applications.

Both B_4C and HEBs possess strong covalent bond characteristics and low self-diffusion coefficients, and the sintering of B_4C and HEB composites remains a challenge requiring very high temperatures. Typical hot pressings at over 2000°C at 30–

40 MPa were used to obtain dense B_4C and HEB composites.[2,17] In this process, HEB phases were formed by sintering of mixed powders of TMB_2s or HEB powders from borothermal (boro/carbothermal) reductions. In comparison, the combination of reaction and sintering in one step has advantages of good sintering ability and less contamination, which enables the ceramics to be densified at temperatures below 1900°C. In addition, the in-situ formed phases are compatible with each other, causing enhanced properties.[18] The in-situ synthesized $(Zr_{0.225}Hf_{0.225}Ta_{0.225}Mo_{0.225}W_{0.1})$ B_2 ceramic via boron-metals reactive spark plasma sintering (RSPS) reached a high hardness of over 27 GPa. However, the reaction between transition metals and boron resulted in coarse microstructures (grain sizes over 10 μm).[19] Previous research has synthesized B_4C-TiB_2 and B_4C-TaB_2 composites with one-step reactive sintering between TiC-B and TaC-B. B_4C and TMB_2s were simultaneously generated and the bulk ceramics have homogeneous and fine microstructures, which are beneficial for enhanced mechanical properties. Moreover, similar thermal expansion coefficients make TMB_2s compatible with B_4C and the incorporation of B_4C improves the hardness and lowers the densities of the composites.[8,20]

In this research, B_4C-45vol.% (TiZrHfNbTa) B_2 composite ceramic was prepared from transition metal carbides (TMCs) and boron powders via one-step RSPS. Phase composition and microstructure evolution of the composite ceramic during the reactive sintering were analyzed by x-ray diffraction, scanning electron microscopy, and energy dispersive x-ray spectroscopy. The effect of microstructure on Vickers hardness, flexural strength, and fracture toughness of as-prepared composite ceramic is discussed and compared with mono-phase HEBs, B_4C, TMB_2-B_4C, and HEB-SiC composite ceramics.

EXPERIMENTAL PROCEDURE

Preparation of B_4C-(TiZrHfNbTa) B_2 Composite Ceramics

Commercial powders of TMCs (TiC, ZrC, HfC, NbC, and TaC with average particle sizes of ~ 1 μm, purity: 99%) and amorphous boron (average particle size: 0.9 μm, purity: 95.8%) were used as raw materials. These powders were weighted according to the following reaction: TMC + 6B = TMB_2 + B_4C and the molar ratios of the five TMCs were equal to obtain B_4C-$(Ti_{0.2}Zr_{0.2}Hf_{0.2}Nb_{0.2}Ta_{0.2})$ B_2 composites. To offset the loss due to reaction with native oxides and subsequent evaporation of boron oxides, 5 wt.% of excess boron was added.

Powders of TMCs and boron were ball mixed in ethanol for 24 h with zirconia balls as the milling medium. The ethanol was removed using a rotary evaporator and the mixtures were dried at 90°C for 24 h. After being passed through a 200 mesh, the mixed powders were loaded into graphite dies and subsequently consolidated into dense cylinders (with dimensions of Φ 30 mm × 4.2 mm) in a spark plasma sintering furnace (SPS-10T-10-IV, Shanghai Chen Hua Electric Furnace Co. Ltd., Shanghai, China) in a 0.1 Pa dynamic vacuum. In order to ensure constant contact of the electrodes with the die/punch set-up, a force of 6 kN was applied during the whole heating and dwelling process. The heating rate was 100°C min^{-1} and a pressure of 40 MPa was applied after the temperature reached 2000°C. After a dwell time of 0–6 min, the pressure was removed in 5 min while the temperature was rapidly cooled around 800°C. When the temperature was below 400°C, the samples were taken out after another 5 min.

CHARACTERIZATION AND TESTING

The relative density (RD) of the composite ceramics were estimated using Archimedes' method with distilled water as the immersing medium. The theoretical density of the HEB phase was an average of the five TMB_2s. The volume fraction of the HEB phase in the composite was estimated as 45%.

Phase compositions of the composite ceramics were determined by x-ray diffraction (XRD, D/max-2200VPC, Rigaku Corporation, Japan) with Cu Kα radiation. The scanning rate was 4° min^{-1}, step 0.02°. Analyses of microstructure and fractured surfaces of the composite ceramic were carried out using scanning electron microscopes (SEM, Thermo Fisher Scientific Apreo C, USA and Hitachi SU5000, Tokyo, Japan), equipped with energy dispersive x-ray spectrometers (EDS, Oxford Instruments plc, UK) for elemental analysis.

The hardness was measured by applying 5 kgf load using a Vickers hardness tester (HVS-30, Shangcai Tester machine Co., Ltd. Shanghai, China). Fracture toughness of the specimen was measured by the indentation method in the Vickers hardness tester by applying 5 kgf load to initiate cracks at the indent corners. The fracture toughness of the specimen was evaluated according to the indentation crack lengths using the formula proposed by Evans and Charles.[21] The reported values were averages of at least 10 indentions.

The flexural strength of the composite was estimated by three-point bending test in a universal testing machine (AGS-X, Shimadzu Co., Kyoto, Japan) with a span of 20 mm and a crosshead speed of 0.5 mm min^{-1}. Test samples with dimensions of 3 mm × 4 mm × 25 mm were used. The reported value of the strength was the average of the best five out of six test bars of composite.

RESULTS

Phase Evolution and Microstructure of B_4C-(TiZrHfNbTa)B_2 Composite

Figure 1 presents the phase compositions of B_4C-HEB composite during the RSPS with varying time. The initial TMCs have almost transformed into di-borides and B_4C after the sintering temperature reached 2000°C. Diffraction peaks are mainly di-boride phases and B_4C phase. Although the molar fraction of B_4C is 50% in the as-synthesized composite, diffraction peaks of B_4C are not conspicuous because of the low x-ray scattering factor of boron and carbon atoms and possible poor crystallinity of the in-situ formed B_4C phase. The peaks of di-boride phases are relatively broad, and there are separate peaks of HfB_2 phase at positions of (001), (101), (110), and (102) planes, implying the formations of various kinds of di-boride phases (and their mutual solid solutions), and a relatively low crystallization degree. With an increasing holding time from 0 min to 3 min at 2000°C, these peaks become sharper, indicating a homogenization of initial formed TMB_2 phases. However, this trend is not obvious when prolonging the holding time from 3 min to 6 min.

With increasing holding time from 1 min to 3 min, the tested RD of the bulk ceramics increases from 85.7 to 96.7 and reaches 97.1% after a 6-min dwelling at 2000°C. Previous studies reported that the formation of solid solution likely promoted densification of ceramics during sintering.[22] With respect to the XRD results, it can be deduced that the formation of the single-phase quinary (TiZrHfNbTa) B_2 solid solution depends on the inter-diffusions between prior generated TMB_2s and/or their mutual solid solutions at elevated temperature. This effect on densification is remarkable in the initial 3 min, but becomes weak during the subsequent dwelling at high temperatures in the present study.

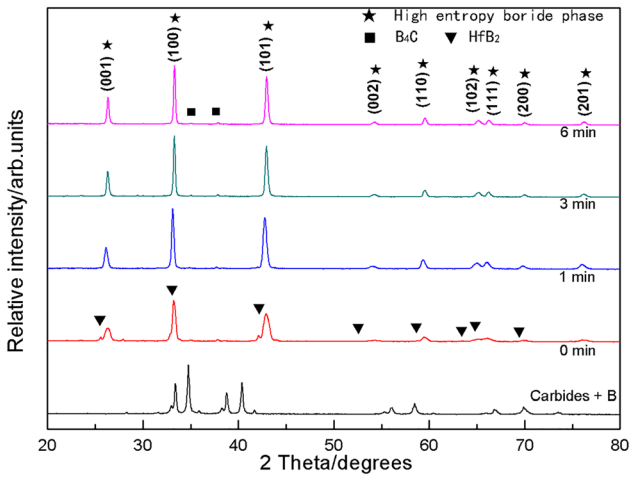

Fig 1. XRD patterns showing phase compositions of the B_4C-(TiZrHfNbTa) B_2 composite ceramic with varying sintering times.

Figure 2 shows backscattered electron (BSE) images of the polished surfaces of the B_4C-HEB composite sintered at 2000°C for 6 min. A dense microstructure is observed for the composite with fine grains. A grain size calculation (see Fig. 2b) from about 400 B_4C grains and 350 HEB grains indicates that the mean sizes of B_4C phase and HEB phase are 0.80 ± 0.35 μm and 0.88 ± 0.48 μm, respectively, and the size of B_4C grains has a narrower distribution than that of HEB phase. The equiaxed B_4C and HEB grains are uniformly distributed, although some aggregations of B_4C and HEB grains were probably caused by uneven mixing of initial powders. Elemental mapping results (see Fig. 3) show that TM elements Ti, Zr, Hf, and Ta have relatively homogeneous distributions, meanwhile segregations of Nb are detected in some locations in the composite. In some HEB or B_4C particles, B_4C or HEB inclusions with nanometer sizes are observed. As the B_4C-TMB_2 binary systems are all eutectic style and the mutual solid solubility limits between B_4C and TMB_2 are very low, these heterogeneous inclusions probably formed by the trapping during the amalgamation and growth of in-situ reaction formed grains.[23–27] Previous results in high-entropy (HfZrTiTaNb) B_2 ceramics have revealed that Nb segregation could be due to low solubility of NbB_2 in other transition metal borides and the slow diffusion of Nb during solid solution formation for HEB ceramics.[13,28] Meanwhile, it was reported that the chemical stability of Nb-B was lower than other metal-boron composites because of the enhanced hybridization between metal and B.[29] Here, in our present study, the segregations of Nb are probably caused by similar effects, and the B_4C phase in the composites further impedes the homogenization of TM elements in HEB grains.

Mechanical Properties of B_4C-(TiZrHfNbTa) B_2 Composite

The tested value of Vickers hardness for a ceramic material generally decreases with increasing test load due to the indentation size effect which results from the proportional specimen resistance.[30] According to the results of Liu et al.[31], the hardness of high-entropy di-boride ceramics reached stable values at critical loads above 49 N (5 kgf). A load of 49 N was therefore used in the present study. The Vickers hardness of B_4C-(TiZrHfNbTa)B_2 ceramic increased from 12.9 ± 0.5 to 19.0 ± 0.9 GPa with increasing sintering time from 1 min to 3 min, and reached 20.9 ± 1.6 GPa after a 6-min sintering. The improvement of the hardness was probably caused by the increase in RD and the solid solution strengthening effect.

The flexural strength of B_4C-(TiZrHfNbTa) B_2 composite ceramic reached 422 ± 48 MPa. The mono-B_4C ceramics had flexural strengths ranging from 300 MPa to 500 MPa.[2] The reported mono-

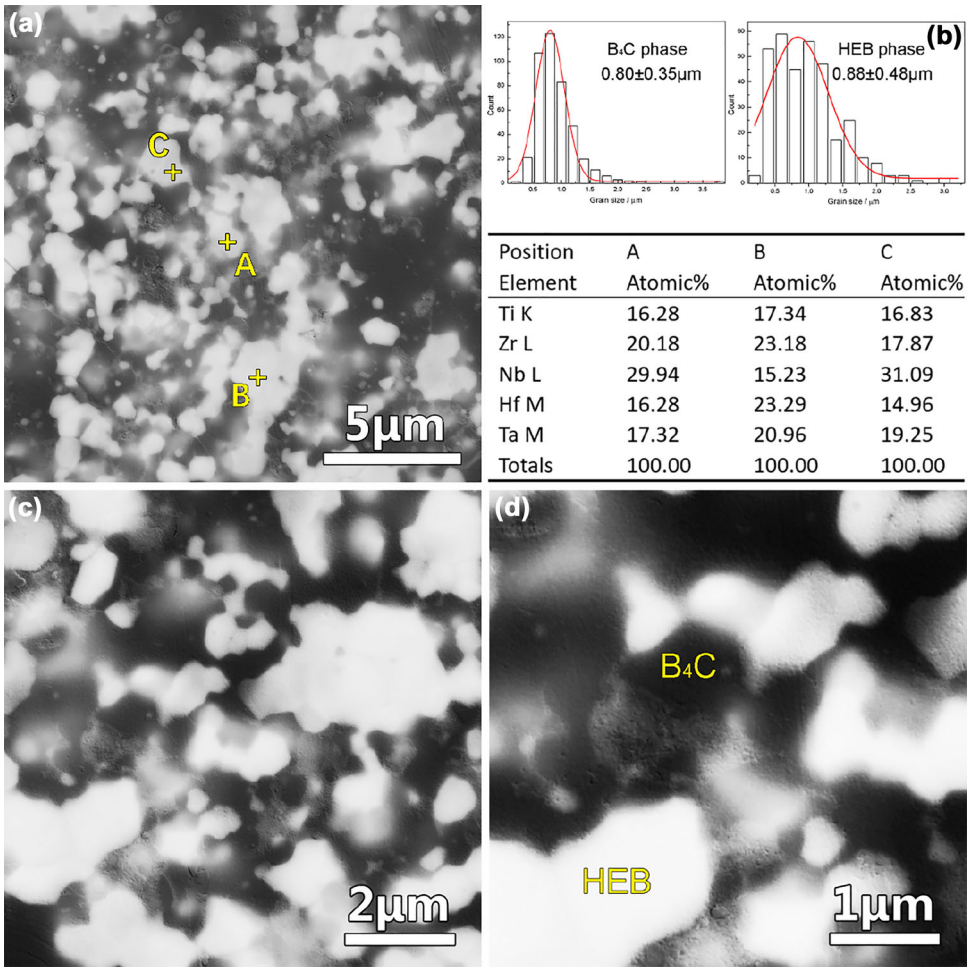

Position	A	B	C
Element	Atomic%	Atomic%	Atomic%
Ti K	16.28	17.34	16.83
Zr L	20.18	23.18	17.87
Nb L	29.94	15.23	31.09
Hf M	16.28	23.29	14.96
Ta M	17.32	20.96	19.25
Totals	100.00	100.00	100.00

Fig 2. BSE images of the polished cross section of the B_4C-(TiZrHfNbTa) B_2 composite ceramic: (a) shows a BSE image of the polished cross section of the composite; (b) presents grain size distributions of B_4C and HEB phases and EDS results at different locations of HEB phase in (a); (c) and (d) are magnified BSE images showing sub-micron sized B_4C and HEB grains.

(TiZrHfNbTa) B_2 ceramic had a flexural strength of 339 MPa.[31] Fracture toughness of B_4C-(TiZrHfNbTa) B_2 composite ceramic was measured as 5.48 ± 0.50 MPa $m^{1/2}$ which was higher than those of B_4C, (TiZrHfNbTa)B_2 ceramics, and RSPS-ed B_4C-TiB_2 ceramic composites.[2,8,31] The incorporation of HEB secondary phase to form composite ceramics has a hybrid strengthening and toughening effect.

Figure 4 shows fractured surfaces of the B_4C-(TiZrHfNbTa) B_2 composite. The sintered bulk ceramic is dense with a few intra-granular pores. B_4C grains present a mainly trans-granular fracture mode, which is consistent with B_4C based ceramics, while HEB grains display both trans-granular and inter-granular modes. The trans-granular type fracture was consistent with those in TMB_2s and HEBs ceramics.[2,8,32] In some large HEB clusters, the inter-granular fracture between some sub-micron sized grains implies relatively weak inter-granular bonding between HEB sub-grains. Some pull-outs of grains were also detected, which is helpful to the fracture toughness of the composite by consuming additional energy to overcome the friction coming from the neighboring grains during the pulling-out process.

Figure 5 presents SEM images of the Vickers hardness indentation on the surface of the B_4C-(TiZrHfNbTa) B_2 composite. The crack propagates tortuously through B_4C particles and the boundaries between B_4C and HEB grains, due to relatively fine grain sizes. The toughening effect of HEB particles by crack deflection, bridging, and branching can be observed and ascribed to the enhancement of the fracture toughness of the composite.

DISCUSSION

Densification Process During the Reactive Sintering

Figure 6a presents the Gibbs energy changes (ΔG) of reactions between boron and TMCs to form TMB_2s and B_4C ranging from 0°C to 2100°C. All five reactions are spontaneous with negative values of ΔG in the temperature range of this investigation. The absolute values of ΔG for reactions of NbC and

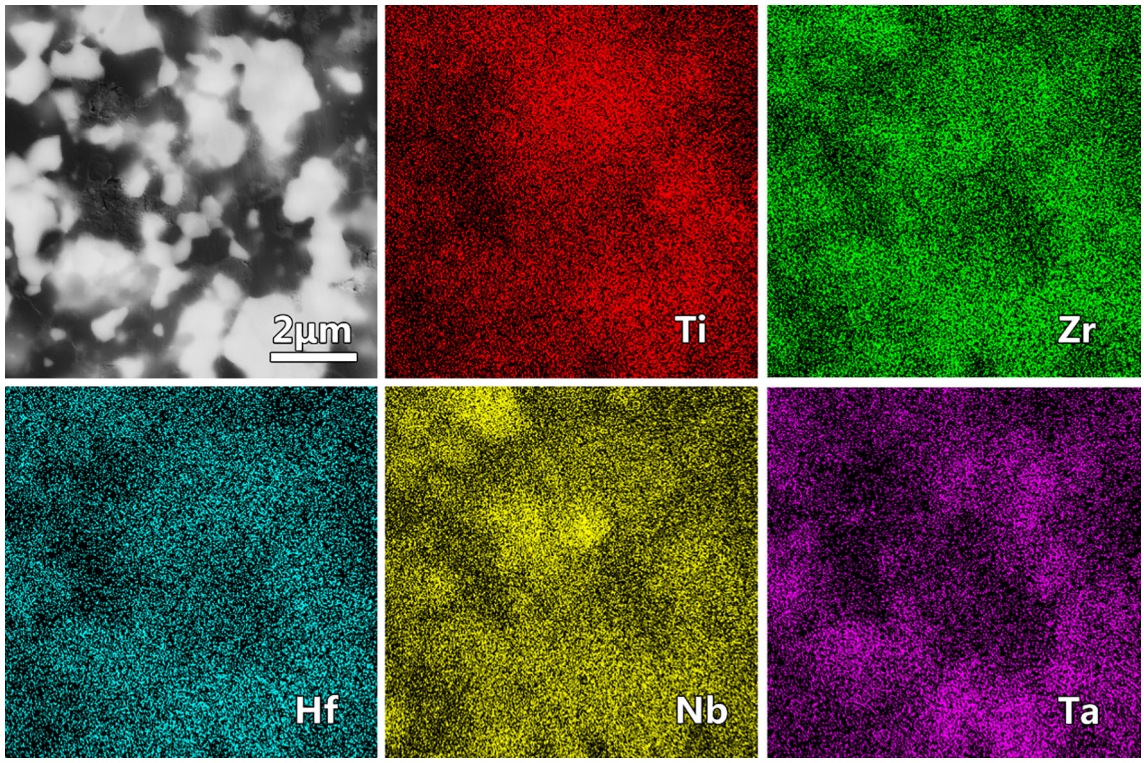

Fig 3. SEM image and corresponding EDS mapping of Ti, Zr, Hf, Nb, and Ta elements showing Nb segregation in HEB phase of the B_4C-(TiZrHfNbTa)B_2 composite.

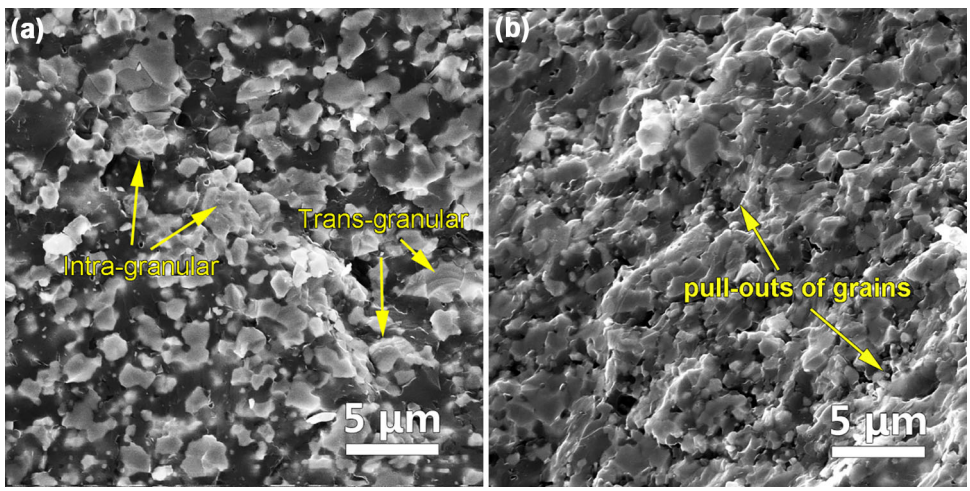

Fig. 4. Fractured surface of the B_4C-(TiZrHfNbTa) B_2 composite: (a) shows mixed intra-granular and trans-granular modes of the composite, (b) shows pull-outs of grains on the fractured surface.

TaC with B to form NbB_2 and TaB_2 are relatively lower than those of group IVB metals. The reaction mechanisms between TMCs and B have been extensively studied. In our present studies, the molar ratio of initial TMCs and B equals 6. The overall reaction takes place under the following sequential steps:

$$TMC + 2B = TMB_2 + C$$

$$C + 4B = B_4C$$

The reactions are so strong that the two associated reactions are thought be simultaneous rather than being divided into detectable steps. Meanwhile, the total volume of the TMB_2s+B_4C products is smaller than that of TMCs+B reactants ($V_{\text{products}} \approx 0.95\ V_{\text{reactants}}$). As a result, the spontaneous reactions enhance the densification process. As the reactions between amorphous B and TMCs proceed,

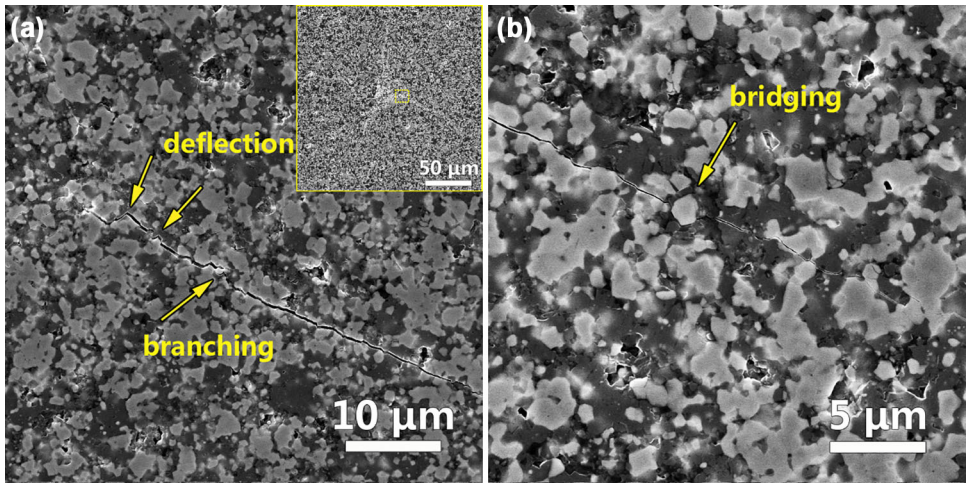

Fig 5. SEM images of the Vickers indention and crack propagation of the B_4C-(TiZrHfNbTa) B_2 composite: (a) crack deflection and branching, (b) crack bridging.

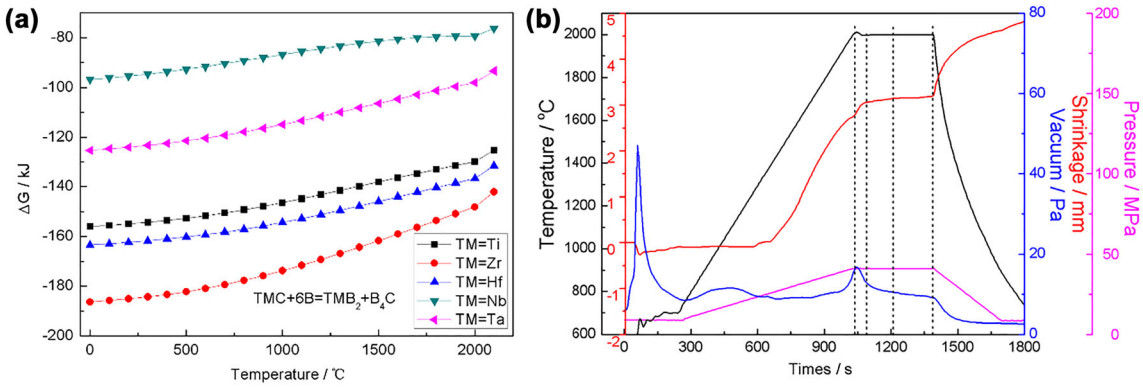

Fig 6. (a) Gibbs energy changes (ΔG) of reactions between boron and TMCs (TM = Ti, Zr, Hf, Nb, and Ta) to form TMB_2s and B_4C at 0–2100°C. (b) Densification behavior of the B_4C-(TiZrHfNbTa) B_2 composite during the RSPS synthesis.

the initial formed TMB_2 grains with different TM atoms form solid solutions with each other. This process is thermodynamically spontaneous with increased entropy of the system.

Figure 6b shows the reactive sintering behavior of B_4C-HEB composite. The shrinkage of the bulk ceramic can be divided into four steps. The shrinkage at the first step between the initial temperature and 1400°C is not conspicuous. In this stage, the solid-state reactions between amorphous B and TMCs are restricted due to relatively low temperatures. Meanwhile, the evaporations of B_2O_3 and other volatile impurities cause a de-densification effect. The second step begins at around 1400°C, the boronizing of TMCs and formation of di-boride solid solutions are the main aspects, both of which effectively promote the densification process. The third stage completes in the first minute of dwelling at 2000°C. The shrinking rate becomes faster after the external pressure reaches the peak value (40 MPa), then it drops at the end of the first minute, and stays nearly at zero until the end of the RSPS. Combined with XRD results, the fourth stage is mainly inter-diffusions and homogenization between TMB_2 solid solutions, which are enhanced under high sintering temperatures, and the peak pressure. However, the almost unchanged shrinkage indicates a prolonged dwelling time over 5 min has little effect on the densification process of the bulk ceramic, which is consistent with the RD result. On the contrary, the grain growth is enhanced at high temperatures, which has also been observed in RSPS-ed B_4C-TiB_2 composites.[8]

Microstructure Evolution During the Reactive Sintering

As mentioned above, the HEB phase in the in-situ B_4C-HEB composite comes from inter-diffusions and homogenization among reaction generated TMB_2s and/or their solid solutions. Lattice parameters of the hexagonal HEB phase were calculated from the XRD patterns at different sintering times to reveal the microstructure evolution during the whole synthesis stage. As the temperature reached 2000°C, the lattice parameters were calculated as a = 3.1095 Å and c = 3.2602 Å. The a value is close to

the average a value (3.110 Å) of the five individual TMB_2,[10] while the c value is less than that of the average c value (3.346 Å), respectively. The a and c values changed to (a = 3.1095 Å, c = 3.2781 Å) and (a = 3.1060 Å, c = 3.3835 Å), after holding at 2000°C for 3 and 6 min, respectively. The values of a and c are compatible with those of previous results reported in (TiZrHfNbTa) B_2 powders and bulk ceramics.[10,28,33–35] The slight decrease in a value and increment in c value are caused by the gradual formation of the quinary solid solution during high-temperature sintering. The more significant variation in the c-axis value than that in the a-axis is caused by the fact that Me-Me bonds in the di-boride lattice can deform more easily perpendicularly to the covalently bonded graphite-like boron network.[36]

The grain sizes of mono-phase B_4C and HEB ceramics by RSPS were calculated as 0.80 ± 0.35 μm and 0.88 ± 0.48 μm, respectively. Such fine grains are beneficial to the mechanical properties of the bulk ceramic. The presence of the B_4C particles has inhibited grain growth in the HEB as has been observed in a recent study of conventional sintering of TMB_2 with B_4C additions. Meanwhile, the presence of TMB_2 grains prevents the grain growth of B_4C.[8,20] It is believed that the HEB and B_4C particles mutually prevent the motion of grain boundaries by the Zener pinning effect during sintering, resulting in an effective inhibition of the grain growth of the two phases in the RSPS-ed composite ceramic. Consequently, relatively fine microstructures (mean grain sizes ~ 1 μm) form. Similar refinement mechanisms have also been utilized in one-step SPS-ed dual-phase HEB-HEC ceramics with mean grain sizes of 5–15 μm,[37] and two-step SPS-ed HEB-SiC ceramics with mean grain sizes of 3–5 μm.[38]

In previous dual-phase HEB-HEC ceramics, the high-entropy phases were derived by inter-diffusions between TMB_2s and TMCs. The mutual pinning effects between HEB and HEC phases were relatively remarkable when the contents of the two phases were comparable, while in HEB-SiC ceramics, SiC was added as second phase particles. The pinning effect of SiC took effect during the high-temperature sintering of the ceramics. In our present B_4C-HEB composite, B_4C and HEB phases were formed via in-situ reactions and the molar ratios of the two were equal. The pinning effect has played roles in not only the initial forming stage of B_4C and HEB particles but also in the following sintering stage. From this view point, the RSPS-ed B_4C-HEB composite from TMC and boron in this study is superior in obtaining finer microstructures compared with composite ceramics from non-reactive sintering.

Effect of Microstructure on Hardness, Strength, and Toughness of the B_4C-(TiZrHfNbTa) B_2 Composite

Table I compiles the test values of Vickers hardnesses of (TiZrHfNbTa) B_2 quintuple di-borides and their composites from the literature. The higher hardness value for the ceramic produced in the present study is attributed to its higher RD, solid solution strengthening, and finer grain size. According to the formula proposed by Engqvist et al.[39], the value of Hv for a composite ceramic increases with the hardness of each component phase and mean free path (λ) value of the composite. The Hv of a high-entropy (TiZrHfNbTa) B_2 phase is higher than the average of five individual TMB_2 ceramics due to a high-entropy effect. The λ value in present B_4C-(TiZrHfNbTa) B_2 ceramic is lower (~ 1 μm) due to the fine grain effect. Consequently, the Hv value is higher than the values of some (TiZrHfNbTa) B_2 ceramics reported in the literature.

The tested flexure strength of the present B_4C-(TiZrHfNbTa)B_2 composite reaches 422 ± 48 MPa, which is about 100 MPa higher than reported values of single phase HEB or B_4C ceramics and comparable to that of an HEB-20vol.%SiC ceramic.[31,40] The tested strength of a monolithic medium-entropy $(Zr_{1/3}Hf_{1/3}Ta_{1/3})B_2$ was 318 MPa with a grain size of about 15 μm while a high-entropy (TiZrHfNbTa) B_2 ceramic had a strength of 339 MPa with a grain size of 4.06 μm.[31,41] From this point of view, the high-entropy effect on the improvement of the strength of (TiZrHfNbTa) B_2 ceramics is relatively weak. The enhanced strength of the HEB-20vol.%SiC composite is probably caused by addition of second phase particles into the high-entropy di-boride ceramic matrix. In the B_4C-(TiZrHfNbTa) B_2 composite, the content of B_4C is ~ 55 vol.%, and the main contribution of the further strength improvement is considered to be the finer grain size of the composite ceramic related to the Hall-Petch relationship:

$$\sigma = \sigma_0 + kD^{-1/2}$$

By reducing the grain sizes of B_4C and HEB phases to sub-micron levels, the strength is enhanced. The tested fracture toughness of B_4C-(TiZrHfNbTa) B_2 composite is remarkably improved compared with both HEB and B_4C ceramics. The toughening mechanisms have two aspects. One is the fine-grain toughening. The fine grains provide more grain boundaries and interfaces between phases, which increases the area of fractured surface and therefore fracture energy for the intergranular part. The other is the introduction of mechanisms such as pull-outs of grains, crack deflection, branching, and bridging by second-phase particles. The mismatch of thermal expansion coefficients between B_4C (5.65×10^{-6} K^{-1}) and HEB (7.815×10^{-6} K^{-1}) phases placed the B_4C grains in compression and HEB grains in tension within the

Table I. Mechanical properties of B_4C-(TiZrHfNbTa) B_2 composite ceramic compared with B_4C- and HEB-based ceramics data from the literature.

Material	RD (%)	Average grain size (μm)	Vickers hardness (GPa)	Flexural strength (MPa)	Fracture toughness (MPa $m^{1/2}$)	References
B_4C	91.22 ± 0.58	1.94	*Hv*1 21.8 ± 1.1	315 ± 25	2.76 ± 0.25	40
B_4C	93.87 ± 0.53	1.6	*Hv*1 26.4 ± 4.3	328 ± 31	3.15 ± 0.23	40
$(ZrHfTa)B_2$	96.99	15 ± 6	*Hv*1 28.6 ± 1.3	318 ± 14	2.9	41
$(TiZrHfNbTa)B_2$	99.8	4.06	*Hv*5 20.2 ± 0.4	339 ± 17	3.81 ± 0.40	31
HEB-20 vol.%SiC	99	HEB: 2.70 SiC: 1.51	*Hv*5 21.4 ± 0.7	447 ± 45	4.85 ± 0.33	31
$(Hf_{0.2}Zr_{0.2}Ti_{0.2}Ta_{0.2}Nb_{0.2})B_2$	92.4		*Hv*0.2 17.5 ± 1.2			10
$(Hf_{0.2}Zr_{0.2}Ti_{0.2}Ta_{0.2}Nb_{0.2})B_2$	99.5	4.9±2.4	*Hv*1 21.0 ± 0.2			45
$(Ti_{0.2}Zr_{0.2}Nb_{0.2}Hf_{0.2}Ta_{0.2})B_2$	~99		*Hv*1 19.4 ± 1.3			37
$(Ti_{0.2}Zr_{0.2}Nb_{0.2}Hf_{0.2}Ta_{0.2})B_2$	94.4	6.67±1.20	*Hv*1 22.44 ± 0.56		2.83 ± 0.15	33
$(Ti_{0.2}Zr_{0.2}Nb_{0.2}Hf_{0.2}Ta_{0.2})B_2$	96.3	1.59	*Hv*0.2 21.7 ± 1.1		4.06 ± 0.35	46
$(Ti_{0.2}Zr_{0.2}Hf_{0.2}Nb_{0.2}Ta_{0.2})B_2$	98.1		*Hv*0.2 20.9 ± 1.1			19
B_4C-$(TiZrHfNbTa)B_2$	97.1	HEB: 0.88 B_4C: 0.80	*Hv*5 20.9 ± 1.6	422±48	5.48 ± 0.50	This work

as-sintered composite.[31,42,43] Stress-induced interfacial micro-cracking results in the weakness of the B_4C/HEB interfaces which therefore enhances crack deflection, branching, and bridging mechanisms.[44]

To summarize the discussion above, the B_4C-(TiZrHfNbTa) B_2 composite produced by the present one-step synthesis has enhanced hardness, flexure strength, and fracture toughness mainly due to high density, the solid solution effect, and fine microstructure.

CONCLUSION

B_4C-45vol.% (TiZrHfNbTa) B_2 composite was fabricated by reactive spark plasma sintering according to the boronation reaction between transition metal carbides and amorphous boron at 2000°C for 6 min. The fabricated composite had a relative density of 97.1% with refined microstructure. The grain sizes of both B_4C and HEB phases were reduced to sub-micron levels by the pinning effect of the in-situ formed second phase. The microstructure with small grain sizes led to the enhanced mechanical properties of the sintered composite ceramic. The Vickers hardness, flexure strength, and fracture toughness reached 20.9 ± 1.6 GPa, 422 ± 48 MPa and 5.48 ± 0.50 MPa $m^{1/2}$, respectively. The toughening mechanisms of crack deflection, branching, and bridging also favored the improvement of fracture toughness.

ACKNOWLEDGEMENTS

This work was financially supported by the National Natural Science Foundation of China (Nos. 52002003, 52072003 and U1860102), Natural Science Foundation of Anhui Province, China (No. 2008085QE196), and Open Fund of Key Laboratory of Green Fabrication and Surface Technology of Advanced Metal Materials (Anhui University of Technology), Ministry of Education (No. GFST2020KF09).

FUNDING

National Natural Science Foundation of China, 52002003, Dong Wang, 52072003, Songlin.Ran, U1860102, Songlin Ran, Natural Science Foundation of Anhui Province, 2008085QE196, Dong Wang, Open fund of Key Laboratory of Green Fabrication and Surface Technology of Advanced Metal Materials (Anhui University of Technology), Ministry of Education, GFST2020KF09, Dong Wang

CONFLICT OF INTEREST

The authors declare that they have no conflicts of interest.

REFERENCES

1. F. Thévenot, *J. Eur. Ceram. Soc.* 6, 205. (1990).
2. A.K. Suri, C. Subramanian, J.K. Sonber, and T.S.R.C. Murthy, *Int. Mater. Rev.* 55, 4. (2010).
3. W. Zhang, S. Yamashita, and H. Kita, *Adv. Appl. Ceram.* 118, 222. (2019).
4. Z. Zhang, X. Du, Z. Li, W. Wang, J. Zhang, and Z. Fu, *J. Eur. Ceram. Soc.* 34, 2153. (2014).
5. L.S. Sigl, *J. Eur. Ceram. Soc.* 18, 1521. (1998).
6. Yu.G. Tkachenko, V.T. Varchenko, V.F. Britun, and D.Z. Yurchenko, *Powder Metall. Met. Ceram.* 44, 245. (2005).
7. Y. Xiong, X. Du, M. Xiang, H. Wang, W. Wang, and Z. Fu, *J. Eur. Ceram. Soc.* 38, 4167. (2018).
8. Z. Liu, D. Wang, J. Li, Q. Huang, and S. Ran, *Scr. Mater.* 135, 15. (2017).
9. X. Cheng, R. He, Z. Qu, S. Ai, and D. Fang, *Ceram. Int.* 41, 14574. (2015).
10. J. Gild, Y. Zhang, T. Harrington, S. Jiang, T. Hu, M.C. Quinn, W.M. Mellor, N. Zhou, K. Vecchio, and J. Luo, *Sci. Rep.* 6, 37946. (2016).
11. C. Oses, C. Toher, and S. Curtarolo, *Nat Rev Mater* 5, 295. (2020).
12. R.-Z. Zhang and M.J. Reece, *J. Mater. Chem. A* 7, 22148. (2019).
13. Y. Zhang, S.-K. Sun, W. Zhang, Y. You, W.-M. Guo, Z.-W. Chen, J.-H. Yuan, and H.-T. Lin, *Ceram. Int.* 46, 14299. (2020).
14. D. Hedman, A.C. Feltrin, Y. Miyamoto, and F. Akhtar, *J. Mater. Sci.* 57, 422. (2022).
15. H. Zhang, D. Hedman, P. Feng, G. Han, and F. Akhtar, *Dalton Trans.* 48, 5161. (2019).
16. H. Zhang and F. Akhtar, *Entropy* 21, 474. (2019).
17. H. Xiang, Y. Xing, F. Dai, H. Wang, L. Su, L. Miao, G. Zhang, Y. Wang, X. Qi, L. Yao, H. Wang, B. Zhao, J. Li, and Y. Zhou, *J. Adv. Ceram.* 10, 385. (2021).
18. S.-K. Sun, G.-J. Zhang, W.-W. Wu, J.-X. Liu, T. Suzuki, and Y. Sakka, *Scripta Mater* 69, 139. (2013).
19. M. Qin, J. Gild, H. Wang, T. Harrington, K.S. Vecchio, and J. Luo, *J. Eur. Ceram. Soc.* 40, 4348. (2020).
20. J. Gu, J. Zou, P. Ma, H. Wang, J. Zhang, W. Wang, and Z. Fu, *J. Mater. Sci. Technol.* 35, 2840. (2019).
21. A.G. Evans and E.A. Charles, *J. Am. Ceram. Soc.* 59, 371. (1976).
22. Y. Zhang, D.-W. Tan, W.-M. Guo, L.-X. Wu, S.-K. Sun, Y. You, H.-T. Lin, and C.-Y. Wang, *J. Am. Ceram. Soc.* 103, 103. (2020).
23. R.M. White and E.C. Dickey, *J. Eur. Ceram. Soc.* 34, 2043. (2014).
24. Q. Yang, C. Hwang, A.U. Khan, V. Domnich, E.D. Gronske, and R.A. Haber, *Mater. Charact.* 155, 109797. (2019).
25. R. Tu, N. Li, Q. Li, S. Zhang, L. Zhang, and T. Goto, *J. Eur. Ceram. Soc.* 36, 3929. (2016).
26. D. Demirskyi and Y. Sakka, *J. Ceram. Soc. Jpn.* 123, 33. (2015).
27. D. Demirskyi, Y. Sakka, and O. Vasylkiv, *J. Am. Ceram. Soc.* 99, 2436. (2016).
28. L. Feng, W.G. Fahrenholtz, G.E. Hilmas, and F. Monteverde, *J. Eur. Ceram. Soc.* 41, 92. (2021).
29. Y. Zhou, H. Xiang, Z. Feng, and Z. Li, *J. Mater. Sci. Technol.* 31, 285. (2015).
30. H. Li and R.C. Bradt, *J. Mater. Sci.* 28, 917. (1993).
31. J.-X. Liu, X.-Q. Shen, Y. Wu, F. Li, Y. Liang, and G.-J. Zhang, *J. Adv. Ceram.* 9, 503. (2020).
32. Y. Zhang, S.-K. Sun, W.-M. Guo, L. Xu, W. Zhang, and H.-T. Lin, *J. Adv. Ceram.* 10, 173. (2021).
33. J. Gu, J. Zou, S.-K. Sun, H. Wang, S.-Y. Yu, J. Zhang, W. Wang, and Z. Fu, *Sci. China Mater.* 62, 1898. (2019).
34. H. Chen, H. Xiang, F.-Z. Dai, J. Liu, and Y. Zhou, *J. Mater. Sci. Technol.* 35, 2404. (2019).
35. F. Monteverde and F. Saraga, *J. Alloy Compd.* 824, 153930. (2020).
36. K.E. Spear, *J. Less Common. Met.* 47, 195. (1976).
37. M. Qin, J. Gild, C. Hu, H. Wang, M.S.B. Hoque, J.L. Braun, T.J. Harrington, P.E. Hopkins, K.S. Vecchio, and J. Luo, *J. Eur. Ceram. Soc.* 40, 5037. (2020).
38. X.-Q. Shen, J.-X. Liu, F. Li, and G.-J. Zhang, *Ceram. Int.* 45, 24508. (2019).
39. H. Engqvist, S. Jacobson, and N. Axén, *Wear* 252, 384. (2002).
40. X. Zhang, Z. Zhang, R. Wen, G. Wang, X. Zhang, J. Mu, H. Che, and W. Wang, *Ceram. Int.* 44, 2615. (2018).
41. D. Demirskyi, T.S. Suzuki, K. Yoshimi, and O. Vasylkiv, *J. Ceram. Soc. Jpn.* 128, 977. (2020).
42. H.J. Klam, H. Hahn, and H. Gleiter, *Acta Metall.* 35, 2101. (1987).
43. G.V. Tsagareishvili, T.G. Nakashidze, J.S. Jobava, G.P. Lomidze, D.E. Khulelidze, D.S. Tsagareishvili, and O.A. Tsagareishvili, *J. Less Common. Met.* 117, 159. (1986).
44. W.S. Rubink, V. Ageh, H. Lide, N.A. Ley, M.L. Young, D.T. Casem, E.J. Faierson, and T.W. Scharf, *J. Eur. Ceram. Soc.* 41, 3321. (2021).
45. L. Feng, F. Monteverde, W.G. Fahrenholtz, and G.E. Hilmas, *Scr. Mater.* 199, 113855. (2021).
46. Y. Zhang, Z.-B. Jiang, S.-K. Sun, W.-M. Guo, Q.-S. Chen, J.-X. Qiu, K. Plucknett, and H.-T. Lin, *J. Eur. Ceram. Soc.* 39, 3920. (2019).